Magnetic Resonance in Medicine 54:1519–1529 (2005)

Tissue Segmentation and Classification of MRSI Data Using Canonical Correlation Analysis

Teresa Laudadio,[1]* Pieter Pels,[2] Lieven De Lathauwer,[1,3] Paul Van Hecke,[4] and Sabine Van Huffel[1]

In this article an accurate and efficient technique for tissue typing is presented. The proposed technique is based on Canonical Correlation Analysis, a statistical method able to simultaneously exploit the spectral and spatial information characterizing the Magnetic Resonance Spectroscopic Imaging (MRSI) data. Recently, Canonical Correlation Analysis has been successfully applied to other types of biomedical data, such as functional MRI data. Here, Canonical Correlation Analysis is adapted for MRSI data processing in order to retrieve in an accurate and efficient way the possible tissue types that characterize the organ under investigation. The potential and limitations of the new technique have been investigated by using simulated as well as in vivo prostate MRSI data, and extensive studies demonstrate a high accuracy, robustness, and efficiency. Moreover, the performance of Canonical Correlation Analysis has been compared to that of ordinary correlation analysis. The test results show that Canonical Correlation Analysis performs best in terms of accuracy and robustness. Magn Reson Med 54:1519–1529, 2005. © 2005 Wiley-Liss, Inc.

Key words: magnetic resonance spectroscopic imaging; canonical correlation analysis; tissue segmentation; classification

Nowadays, MRSI represents a powerful non-invasive diagnostic tool. The ability of Magnetic Resonance Spectroscopy to detect metabolites is already very useful in daily radiologic practice since it provides significant biochemical information on the molecules of the organism under investigation. MRSI data can also be exploited in tissue segmentation techniques, which play a crucial role in many biomedical applications, such as the quantification of tissue volumes, localization of possible pathologies, improvement of pre-surgical diagnosis, and optimization of the surgical approach, therapy planning, etc. A variety of methods are available in the literature. They are often used in combination in order to solve different segmentation problems.

They can be divided into several categories: thresholding techniques (1), region growing techniques (2), clustering techniques (3), Markov random field models (4), classifiers (5), artificial neural networks (6), etc. In this article, a fast and reliable tissue segmentation technique, based on a statistical method called Canonical Correlation Analysis (CCA), is proposed. This method is the multivariate variant of the ordinary correlation analysis and has already been successfully applied to functional Magnetic Resonance Imaging data in order to map sensor, motor, and cognitive functions to specific areas in the brain (7). Here CCA is adapted for MRSI data processing in order to detect possible homogeneous tissue regions, such as tumor regions, characterizing the considered sample. The goal is achieved by combining the spectral-spatial information provided by the MRSI data set and a signal subspace that models the spectrum of a characteristic tissue type, which may be present in the organ under investigation and, therefore, needs to be detected. More precisely, CCA quantifies the relationship between two sets of variables, magnitude spectra of the measured data and signal subspace, by means of correlation coefficients. These coefficients are afterward exploited in order to construct nosologic images (8) in which all the detected tissues are visualized. Such images can be easily interpreted by radiologists and physicians and, along with clinical and radiologic information, can improve the accuracy of the diagnosis.

Extensive studies, performed on simulated as well as in vivo prostate MRSI data, were carried out in order to explore the properties of the proposed method. Moreover, the performance of CCA and ordinary correlation analysis was compared. The aforementioned studies show that CCA significantly outperforms ordinary correlation analysis in terms of accuracy and robustness.

The article is organized as follows. In the Theory section, the basic definition of CCA is introduced and 3 possible implementations are outlined. In the Methods section, the application of CCA to MRSI data is described and the set up for the simulation studies and the acquisition environment of the in vivo studies is defined. In the Results and Discussion section, the results of the simulation and in vivo studies are reported and discussed. Finally, in the Conclusions section, the main conclusions are formulated.

[1]Department of Electrical Engineering, Division ESAT-SCD, Katholieke Universiteit Leuven, Leuven-Heverlee, Belgium.

[2]Department of Radiology, University of California, San Francisco, CA, USA.

[3]ETIS (CNRS, ENSEA, UCP), Centre National de la Recherche Scientifique, Cergy-Pontoise, France.

[4]Biomedical NMR Unit, O & N Gasthuisberg, Katholieke Universiteit Leuven, Leuven, Belgium.

Grant Sponsor: Research Council KUL; Grant Numbers: GOA-MEFISTO 666, GOA-AMBioRICS, several Ph.D./postdoc and fellow grants. Grant Sponsor: Flemish Government: FWO; Grant Numbers: Ph.D./postdoc grants, projects, G.0407.02 (support vector machines), G.0269.02 (magnetic resonance spectroscopic imaging), G.0270.02 (nonlinear Lp approximation), G.0360.05 (EEG signal analysis for epilepsy monitoring), research communities (ICCoS, ANMMM). Grant Sponsor: IWT; Grant Numbers: Ph.D. Grants. Grant Sponsor: Belgian Federal Government; Grant Numbers: DWTC (IUAP IV-02 (1996–2001) and IUAP V-22 (2002–2006): Dynamical Systems and Control: Computation, Identification & Modeling)). Grant Sponsor: EU: PDT-COIL; Grant Number: NNE5/2001/887; BIOPATTERN, Grant Number: FP6–2002-IST 508803; ETUTUMOUR, Grant Number: FP6–2002-LIFESCIHEALTH 503094.

*Correspondence to: Teresa Laudadio, Department of Electrical Engineering, Division ESAT-SCD, Katholieke Universiteit Leuven, Kasteelpark Arenberg 10, 3001 Leuven-Heverlee, Belgium. E-mail: laudadio@esat.kuleuven.ac.be

Received 2 May 2005; revised 26 July 2005; accepted 12 August 2005.

DOI 10.1002/mrm.20710

Published online 7 November 2005 in Wiley InterScience (www.interscience.wiley.com).

© 2005 Wiley-Liss, Inc.

THEORY

CCA is a statistical technique developed by Hotelling in 1936 in order to assess the relationship between 2 sets of variables (9). It is a multichannel generalization of ordinary correlation analysis, which quantifies the relationship between 2 random variables x and y by means of the so-called correlation coefficient ρ:

$$\rho = \frac{Cov[x, y]}{\sqrt{V[x]V[y]}} \quad [1]$$

where Cov and V stand for covariance and variance, respectively. The correlation coefficient ρ is a scalar with value between –1 and 1 that measures the degree of linear dependence between x and y. For zero-mean variables, Eq. [1] is replaced by:

$$\rho = \frac{E[xy]}{\sqrt{E[x^2]E[y^2]}} \quad [2]$$

where E stands for expected value. Canonical correlation analysis can be applied to multichannel signal processing as follows: consider 2 zero-mean multivariate random vectors $x = [x_1(t), \ldots, x_m(t)]^T$ and $y = [y_1(t), \ldots, y_n(t)]^T$, with $t = 1,\ldots,N$, where the superscript T denotes the transpose. The following linear combinations of the components in x and y are defined, which respectively represent 2 new scalar random variables X and Y:

$$\begin{aligned} X &= \omega_{x_1}x_1 + \cdots + \omega_{x_m}x_m = \omega_x^T x \\ Y &= \omega_{y_1}y_1 + \cdots + \omega_{y_n}y_n = \omega_y^T y \end{aligned} \quad [3]$$

CCA computes the linear combination coefficients $\omega_x = [\omega_{x_1}, \ldots, \omega_{x_m}]^T$ and $\omega_y = [\omega_{y_1}, \ldots, \omega_{y_n}]^T$, called regression weights, so that the correlation between the new variables X and Y is maximum. The solution $\omega_x = \omega_y = 0$ is not allowed, and the new variables X and Y are called canonical variates. The regression weights are found by solving the maximization problem obtained by substituting Eqs. [3] into Eq. [2], i.e.

$$\max_{\omega_x,\omega_y} \rho(\omega_x, \omega_y) = \frac{\omega_x^T C_{xy}\omega_y}{\sqrt{(\omega_x^T C_{xx}\omega_x)(\omega_y^T C_{yy}\omega_y)}} \quad [4]$$

where C_{xx} and C_{yy} are the within-set covariance matrices of x and y, respectively, and C_{xy} is the between-sets covariance matrix. In practice, estimated covariance matrices are used:

$$\begin{aligned} \hat{C}_{xx} &= \frac{1}{N}\sum_{t=1}^{N} x(t)x(t)^T \\ \hat{C}_{yy} &= \frac{1}{N}\sum_{t=1}^{N} y(t)y(t)^T \\ \hat{C}_{xy} &= \frac{1}{N}\sum_{t=1}^{N} x(t)y(t)^T \end{aligned} \quad [5]$$

The maximization problem is solved by setting the derivatives of Eq. [4], with respect to ω_x and ω_y, equal to zero, resulting in the following system of equations:

$$\begin{cases} \hat{C}_{xy}\hat{\omega}_y = \rho\lambda_x\hat{C}_{xx}\hat{\omega}_x \\ \hat{C}_{yx}\hat{\omega}_x = \rho\lambda_y\hat{C}_{yy}\hat{\omega}_y \end{cases} \quad [6]$$

where $\lambda_x = \lambda_y^{-1} = \sqrt{(\hat{\omega}_y^T\hat{C}_{yy}\hat{\omega}_y)/(\hat{\omega}_x^T\hat{C}_{xx}\hat{\omega}_x)}$ are scaling factors. By combining the two equations in Eq. [6], the following eigenvalue problems are obtained:

$$\begin{cases} \hat{C}_{xx}^{-1}\hat{C}_{xy}\hat{C}_{yy}^{-1}\hat{C}_{yx}\hat{\omega}_x = \rho^2\hat{\omega}_x \\ \hat{C}_{yy}^{-1}\hat{C}_{yx}\hat{C}_{xx}^{-1}\hat{C}_{xy}\hat{\omega}_y = \rho^2\hat{\omega}_y \end{cases} \quad [7]$$

whose common eigenvalues ρ^2 represent the squared canonical coefficients between x and y. The first pair of canonical variates correspond to the eigenvectors $\hat{\omega}_x$ and $\hat{\omega}_y$ associated with the largest eigenvalue. The remaining canonical variates correspond to the remaining eigenvectors, and the associated eigenvalues are the squared canonical coefficients. It can be shown that the canonical variates are maximally correlated and, at the same time, uncorrelated with the previous pairs. As can be observed in Eq. [7], matrix inversions need to be performed. These operations could lead to numerical instability if $\hat{C}_{xx}$ and $\hat{C}_{yy}$ are almost rank deficient. Two more reliable algorithms are described in (10) and (11), respectively. The first algorithm computes the canonical coefficients and the corresponding regression weights by solving a generalized symmetric eigenvalue problem. The second algorithm is based on the computation of the principal angles. In fact, canonical correlation analysis is the statistical interpretation of the geometric tool principal angles between linear subspaces and associated principal directions (9). Here, an outline for both algorithms is provided.

Algorithm CCA-GEP: CCA by Solving a Generalized Eigenvalue Problem (GEP)

Given the zero-mean multivariate random vectors $x = [x_1(t), \ldots, x_m(t)]^T$ and $y = [y_1(t), \ldots, y_n(t)]^T$, with $t = 1,\ldots,N$

- Step 1. Compute the estimated covariance matrices $\hat{C}_{xx}$, $\hat{C}_{yy}$, and $\hat{C}_{xy}$.
- Step 2. Solve the following generalized symmetric eigenvalue problem

$$\begin{bmatrix} 0 & \hat{C}_{xy} \\ \hat{C}_{xy}^T & 0 \end{bmatrix}\begin{bmatrix} \hat{\omega}_x \\ \hat{\omega}_y \end{bmatrix} = \begin{bmatrix} \hat{C}_{xx} & 0 \\ 0 & \hat{C}_{yy} \end{bmatrix}\begin{bmatrix} \hat{\omega}_x \\ \hat{\omega}_y \end{bmatrix}\rho \quad [8]$$

subject to $\hat{\omega}_x^T\hat{C}_{xx}\hat{\omega}_x = 1$ and $\hat{\omega}_y^T\hat{C}_{yy}\hat{\omega}_y = 1$.

- Step 3. Set the canonical coefficients equal to the eigenvalues ρ, and the regression weights equal to the corresponding eigenvectors $\hat{\omega}_x$ and $\hat{\omega}_y$.

Algorithm CCA-PA: CCA by Computing Principal Angles (PA)

Given the zero-mean multivariate random vectors $x = [x_1(t), \ldots, x_m(t)]^T$ and $y = [y_1(t), \ldots, y_n(t)]^T$, with $t = 1,\ldots,N$.

- Step 1. Consider the matrices $\tilde{X}$ and $\tilde{Y}$, defined as follows:

$$\tilde{X} = \begin{bmatrix} x_1(1) & \cdots & x_m(1) \\ \vdots & & \vdots \\ x_1(N) & \cdots & x_m(N) \end{bmatrix},$$

$$\tilde{Y} = \begin{bmatrix} y_1(1) & \cdots & y_n(1) \\ \vdots & & \vdots \\ y_1(N) & \cdots & y_n(N) \end{bmatrix} \quad [9]$$

- Step 2. Compute the QR decompositions (12) of $\tilde{X}$ and $\tilde{Y}$:

$$\begin{cases} \tilde{X} = Q_{\tilde{X}} R_{\tilde{X}} \\ \tilde{Y} = Q_{\tilde{Y}} R_{\tilde{Y}} \end{cases} \quad [10]$$

where $Q_{\tilde{X}}$ and $Q_{\tilde{Y}}$ are orthogonal matrices and $R_{\tilde{X}}$ and $R_{\tilde{Y}}$ are upper triangular matrices.

- Step 3. Compute the Singular Value Decomposition (12) of $Q_{\tilde{X}}^T Q_{\tilde{Y}}$:

$$Q_{\tilde{X}}^T Q_{\tilde{Y}} = USV^T \quad [11]$$

where S is a diagonal matrix and U and V are orthogonal matrices. The cosines of the principal angles are given by the diagonal elements of S.

- Step 4. Set the canonical coefficients equal to the diagonal elements of the matrix S and compute the corresponding regression weights as $\omega_{\tilde{X}} = R_{\tilde{X}}^{-1} U$ and $\omega_{\tilde{Y}} = R_{\tilde{Y}}^{-1} V$.

The computation of the principal angles yields the most robust implementation of CCA, since it is able to provide reliable results even when the matrices $\tilde{X}$ and $\tilde{Y}$ are singular. A comparison of the last two implementations in terms of computational efficiency is reported in the Results section.

METHODS

CCA Applied to MRSI Data

During the MRSI data acquisition procedure, a number of image slices is acquired. Each image can be partitioned into a certain number of volume elements, called voxels, each characterized by a time-domain signal of length N. In the proposed tissue segmentation approach, the aim is to detect those voxels whose spectra correlate best with model tissue spectra, which are defined a priori. When applying correlation analysis to MRSI data, the variables x and y need to be specified. In ordinary correlation analysis, x and y are univariate variables and, specifically, the x variable consists of the magnitude spectrum of the measured signal contained in each voxel, while the y variable consists of the model tissue magnitude spectrum. The correlation coefficient between x and y is computed and, afterward, assigned to the voxel under investigation. Once each voxel has been processed, a new grid of voxels, of the same size of the original image, is obtained, which contains correlation coefficients instead of MRSI signals. This new grid is called a correlation map.

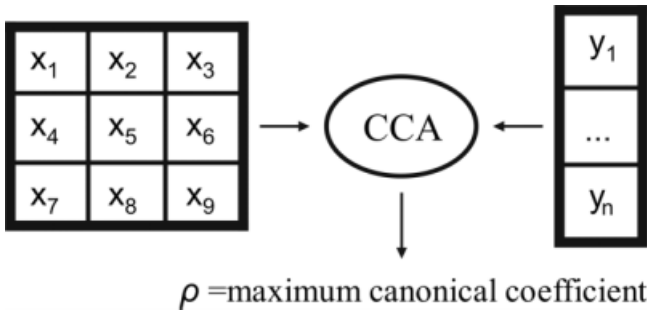


FIG. 1. CCA applied to a 3 × 3 region of voxels in the MRS image and a set of n spectral basis functions.

The difference between ordinary correlation analysis and CCA mainly consists in a different choice of the variables x and y. In fact, in order to compute the correlation maps, it is possible to exploit the spatial information characterizing the MRSI data set by considering, as variable x, a multivariate vector with components representing the magnitude spectrum characterizing the considered voxel as well as the magnitude spectra contained in the neighbor voxels. Several spatial models can be adopted for choosing the neighbor voxels, typical examples of which are described in (7). The variable y also consists of a multivariate vector. Its components represent the basis functions of a signal subspace, which models the characteristic tissue magnitude spectrum we are looking for and its possible variations (in amplitudes, frequency shifts, and damping factors) that normally affect realistic MRSI data. Several approaches can be adopted in order to model a proper signal subspace; an exhaustive overview is given in (7). Once the x and y variables have been defined, CCA is applied voxel by voxel and the largest canonical coefficient is assigned to the voxel under investigation, so that a correlation map is obtained as in the ordinary correlation analysis case. Figure 1 schematically shows the CCA approach when processing a 3 × 3 voxel region containing the magnitude spectrum x_5 along with its neighbor magnitude spectra. In this particular spatial model, called the "3 × 3 model," the variable x contains 9 components, namely, $x = [x_1, \ldots, x_9]^T$.

Simulation Studies

Figure 2 shows the magnitude spectra of 4 different simulated signals, derived from in vivo data measured in the human prostate, representing, from top to bottom, very aggressive tumor tissue, moderately aggressive tumor tissue, mixed tumor tissue, and healthy peripheral zone tissue. As can be observed in the above mentioned Figure, the spectra are characterized by the presence of 3 metabolite peaks: Choline, Creatine, and Citrate doublet. In particular, aggressive tumor tissue is characterized by a strong contribution of Choline, while healthy tissue exhibits a higher contribution of Citrate. In general, prostate tumor regions are characterized by higher levels of Choline and reduced levels of Citrate. The spectra represent the Dis-

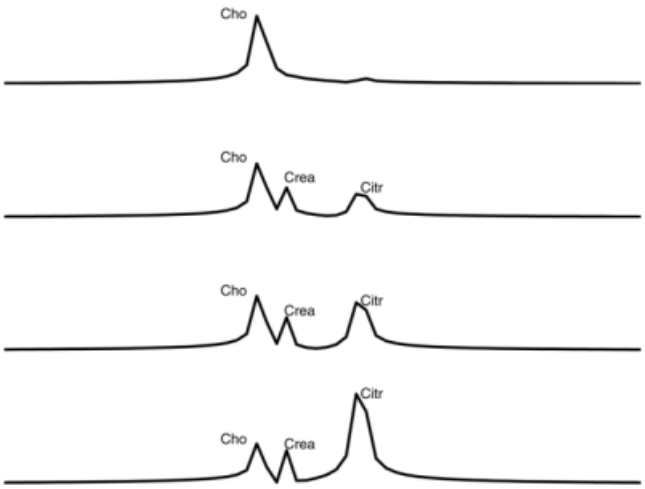


FIG. 2. Magnitude spectra of characteristic prostate signals. From top to bottom: aggressive tumor tissue spectrum; moderately aggressive tumor tissue spectrum; mixed tumor tissue spectrum; healthy tissue spectrum. The spectra contain the following compounds: Choline (Cho), Creatine (Crea), and Citrate doublet (Citr).

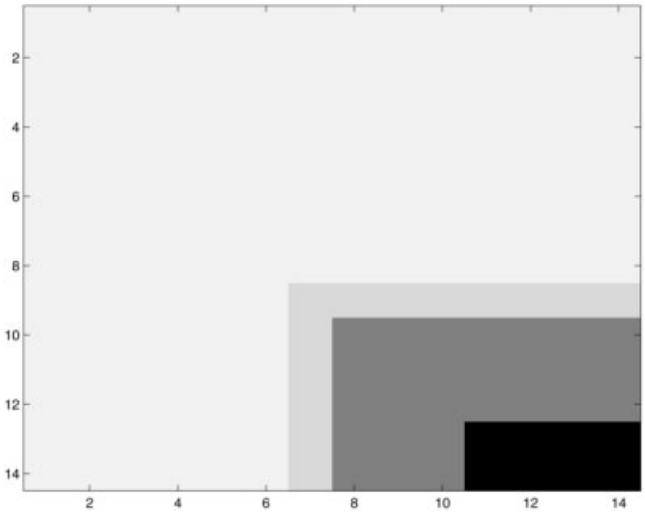


FIG. 3. Original tissue grid. Black region: aggressive tumor voxels; dark gray region: moderately aggressive tumor voxels; gray region: mixed tissue voxels; light gray region: healthy tissue voxels.

crete Fourier Transform of 4 signals consisting of 256 complex data points ($N = 256$) modeled as the sum of $K = 4$ exponentially damped complex sinusoids:

$$s_n = \sum_{k=1}^{K} a_k e^{j\varphi_k} e^{(-d_k + j2\pi f_k)t_n}, \quad n = 1, \ldots, N \qquad [12]$$

where s_n represents the n-th data point of the simulated signal; $j = \sqrt{-1}$ represents the imaginary unit; the parameters a_k, φ_k, d_k, and f_k denote the amplitude, phase, damping factor, and frequency, respectively; and $t_n = t_o + n\Delta t$, with Δt the sampling interval and t_o the time between the effective time origin and the first data point to be included in the analysis. The parameter values of the noiseless simulated signals are reported in Table 1. The dampings and frequencies were selected based on in vivo prostate data acquired at 1.5T. The Citrate was modeled as a doublet with frequency split equal to 2.5Hz. The amplitude values are expressed in arbitrary units (a.u.).

A simulated MRSI data set was produced, consisting of a 14 × 14 grid of voxels, in which 4 different and well localized regions of tissue spectra were inserted. The grid is shown in Fig. 3, and the tissue regions are indicated by different colors: black for aggressive tumor tissue, dark gray for tumor tissue, gray for mixed tissue, and light gray for healthy tissue. Figure 4 shows the magnitude spectra contained in the previous grid. In order to simulate a realistic MRSI data set, variations were introduced on the signal parameters displayed in Table 1. More precisely, spectra for each type of tissue were generated, randomly characterized by variations up to 20% for amplitudes, up to 40 times the given value for the damping factors, up to a shift of 1.25Hz for the frequencies. The magnitude spectra of the simulated signals were perturbed by adding Gaussian noise with SD σ. Ordinary correlation analysis and CCA were then applied in order to detect the 4 tissue regions.

Choice of the Spatial Model

As already mentioned in the previous section, several spatial models can be chosen when applying CCA. As a particular case, the ordinary correlation analysis can be considered as a single-voxel model. The performance of the following spatial models was investigated:

the single-voxel model
the 3 × 3 model (Fig. 1)
the 3 × 3 model without corner voxels ($x = [x_2, x_4, x_5, x_6, x_8]^T$)
the symmetric 3 × 3 model ($x = [x_5, (x_1 + x_9)/2, (x_2 + x_8)/2, (x_3 + x_7)/2, (x_4 + x_6)/2]^T$)

Table 1
Parameter Values of the Noiseless Simulated Signals

Parameters	Choline	Creatine	Citrate 1	Citrate 2
Frequency	−49.3 Hz	−38.9 Hz	−12.1 Hz	−9.6 Hz
Damping	2 Hz	2 Hz	2 Hz	2 Hz
Phase	0°	0°	0°	0°
Amplitude aggressive tumor	4.3e6 a.u.	0.2e6 a.u.	0.2e6 a.u.	0.2e6 a.u.
Amplitude tumor	3.3e6 a.u.	1.6e6 a.u.	1.2e6 a.u.	1.2e6 a.u.
Amplitude mixed tissue	3.3e6 a.u.	1.8e6 a.u.	2.4e6 a.u.	2.4e6 a.u.
Amplitude healthy tissue	2.3e6 a.u.	1.8e6 a.u.	4.4e6 a.u.	4.4e6 a.u.

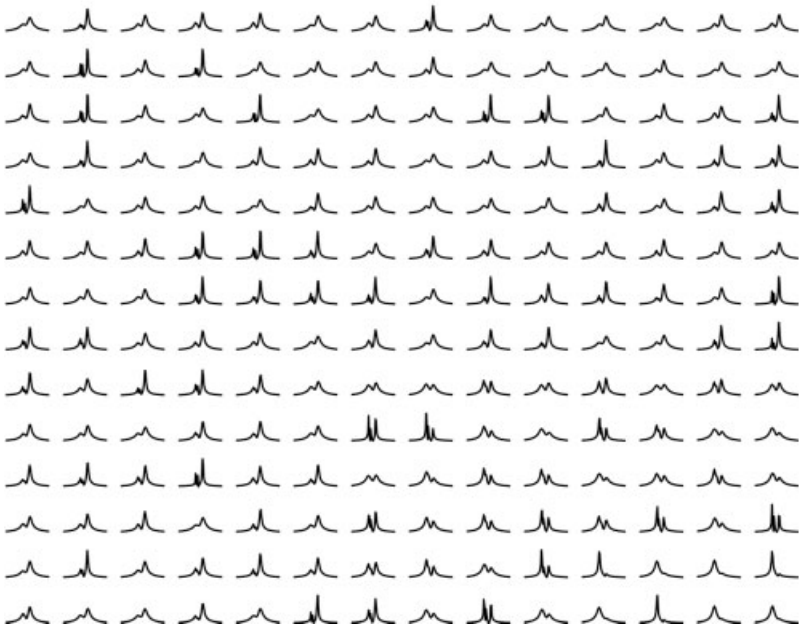


FIG. 4. Magnitude spectra of the noiseless simulated MRSI data.

the symmetric 3 × 3 model without corner voxels ($x = [x_5, (x_2 + x_8)/2, (x_4 + x_6)/2]^T$)

The obtained results are described in the "Results" section.

Choice of the Subspace Model

Concerning the choice of the *y* variable, two different approaches were considered in order to define the proper signal subspace able to model the characteristic tissue spectra and their possible variations. Specifically, the Taylor model and the Principal Component Analysis model (PCA) were considered and compared. In order to define the first component of the variable *y*, 2000 signals, characterized by realistic variations of the noiseless simulated signal parameters, were generated. The first component of the *y* variable was then defined as the mean of the magnitude spectra of the generated signals for both approaches. In the Taylor approach, the second component of *y* was obtained as the first-order derivative of the first component, approximated by first-order finite differences. The first Principal Component of the matrix containing the mean-centered magnitude spectra of the signals was chosen as the second component for the PCA model. For the sake of clarity, the procedure to compute the aforementioned subspace models is here outlined.

The Taylor Subspace Model

- Compute the simulated noiseless signal corresponding to the considered tissue type (with parameters reported in Table 1) and its magnitude spectrum $S(\omega_n)$, where ω_n represents the frequency and $n = 1,\ldots,N$.
- Produce a high number M of signals by introducing realistic variations on the noiseless signal parameters of the chosen tissue type.
- Compute the magnitude spectra $S_i(\omega_n)$, $i = 1,\ldots,M$, of the M signals produced in the previous step.
- Set the components of the variable *y* as:

$$\begin{cases} y_1(n) = \dfrac{1}{M}\displaystyle\sum_{i=1}^{M} S_i(\omega_n) \\ y_2(n) = \dfrac{S(\omega_{n+1}) - S(\omega_n)}{\Delta\omega} \end{cases} \quad [13]$$

where $\Delta\omega$ is the sampling frequency.

The PCA Subspace Model

- Compute the simulated noiseless signal corresponding to the considered tissue type (with parameters reported in Table 1) and its magnitude spectrum $S(\omega_n)$, where ω_n represents the frequency and $n = 1,\ldots,N$.
- Produce a high number M of signals by introducing realistic variations on the noiseless signal parameters of the chosen tissue type.
- Compute the magnitude spectra $S_i(\omega_n)$, $i = 1,\ldots,M$, of the M signals produced in the previous step and arrange them as rows into a matrix D.
- Perform Principal Component Analysis on the matrix D and denote the first Principal Component as 1^{st} *PC*.
- Set the components of the variable *y* as:

$$\begin{cases} y_1(n) = \dfrac{1}{M}\displaystyle\sum_{i=1}^{M} S_i(\omega_n) \\ y_2(n) = 1^{st}PC \end{cases} \quad [14]$$

Concerning the choice of the *y* variable for the single voxel approach, only one component was considered and set

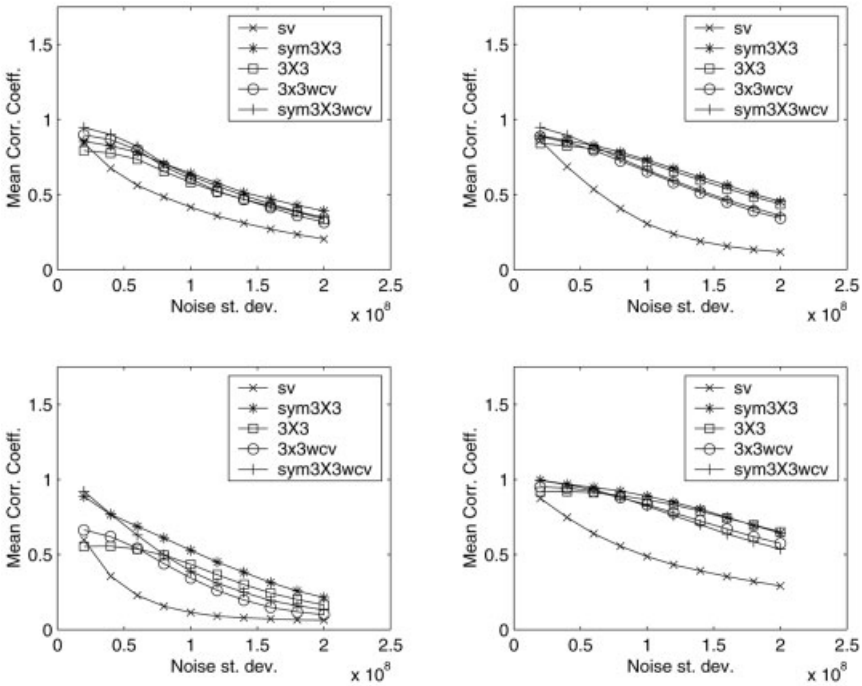


FIG. 5. Mean of the correlation coefficients, over 300 simulation runs, between the detected regions and the original tissue regions as a function of the SD, when considering different spatial models. Subspace model: PCA. Top: aggressive tumor (left), moderately aggressive tumor (right). Bottom: mixed tissue (left), healthy tissue (right).

equal to the first component of the Taylor and PCA subspace models, namely $y = y_1(n)$.

In Vivo Studies

CCA and ordinary correlation analysis were applied to in vivo prostate MRSI data. The data were acquired in the Radiology Department of the K. U. Leuven University Hospital, as part of the routine clinical preoperative MR imaging and spectroscopy protocol for the prostate. They were acquired at 63.6 MHz on a 1.5T Siemens Sonata scanner, using a 3D PRESS CSI sequence (TR = 600 ms, TE = 100 ms). The FOV was adapted to the PRESS box surrounding the prostate that was positioned such as to suppress unwanted fat signals around the prostate. The CSI FOV and matrix size were set to obtain isotropic voxels at acquisition (typ. 6 mm × 6 mm × 6 mm). The data were reconstructed to a 16 × 16 × 16 3D matrix. Each CSI voxel signal consists of 512 complex data points in the time domain and the sampling time is 0.8 ms. The acquisition averages responded to a weighted *k*-space sampling scheme so as to obtain a substantial gain in S/N within a short time, without affecting dramatically the spatial resolution. The total 3D volume was acquired in about 11 min. The coil was an intrarectal coil for maximal S/N in both images and spectra. All patients signed an informed consent paper, in agreement with the guidelines of the University Hospital Ethical Committee. In the considered example, the slice of interest is slice number 8.

RESULTS AND DISCUSSION

Simulation Results

In the simulation studies, 300 simulation runs were performed for different noise SD values. Before applying the proposed tissue segmentation method, 4 different *y* variables were defined, one for each prostate tissue type. CCA was then applied between the noisy data set and the above mentioned *y* variables, and 4 correlation maps were obtained. The nosologic image, as defined in (8), consisting of one single image in which all the detected tissue types are visualized, was obtained by comparing, voxel by voxel, the 4 canonical coefficients characterizing the different correlation maps. The considered voxel was then assigned to the tissue with the highest canonical coefficient and labeled by the corresponding tissue color.

In order to compare the performance of CCA when applying different spatial models and/or different subspace models, the correlation coefficients between the original and the detected tissue regions were estimated for each simulation run. Figure 5 shows the mean value of these correlation coefficients, over the total number of simulation runs and for each noise level, when considering the PCA subspace model. Different spatial models were applied, namely, the single voxel approach (sv), the symmetric 3 × 3 model (sym3 × 3), the 3 × 3 model (3 × 3), the 3 × 3 model without corner voxels (3 × 3wcv), and the symmetric 3 × 3 model without corner voxels (sym3 × 3wcv). As can be observed in the Figure, the best performance is obtained for the symmetric 3 × 3 model, while the single voxel model is least accurate, especially for high noise levels. In general, the performance of all models is sensitive to the number of voxels characterizing the original tissue region as well as to the shape of the spectra. In fact, the quality of the performance for the mixed tissue region is much poorer with respect to the performance shown for the other tissue regions, since little spatial information can be exploited and since the level of the different metabolites in the spectra is not as discriminating as in the other tissue spectra. In Fig. 6 (left) the mean value of the computation time (in seconds), as a function of the

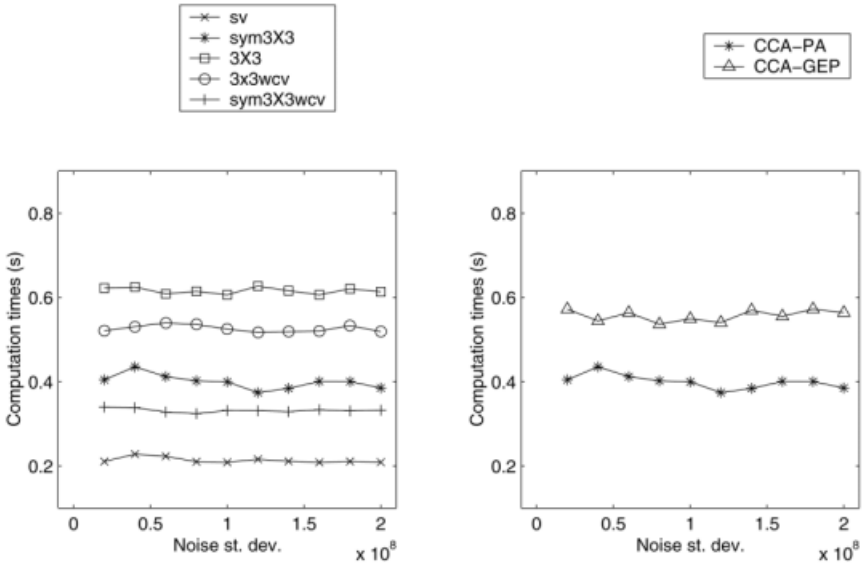


FIG. 6. Mean of the computation times (in seconds), over 300 simulation runs and as a function of the SD. Left: the PCA subspace model and different spatial models are applied. Right: the CCA implementations based on the computation of the principal angles (CCA-PA) and on solving a generalized eigenvalue problem (CCA-GEP) are applied. Spatial model: symmetric 3×3. Subspace model: PCA.

noise SD and over the total number of simulation runs, is displayed. The single voxel model is the most efficient, but the other models can be considered efficient as well since they need less than 1 s for processing the whole simulated MRSI data set.

Extensive studies were also carried out in order to compare the performance of the PCA and Taylor subspace models. The two approaches showed a similar behavior in terms of accuracy as well as in terms of computational efficiency, since they exploit the same number of components in the variable x and y.

Figure 6 (right) shows the computation time versus the noise SD, over the total number of simulation runs, of the CCA implementations based on solving a symmetric generalized eigenvalue problem (CCA-GEP, Eq. [8]) and on computing principal angles (CCA-PA, Eq. [11]), respectively. As can be observed in the Figure, the latter implementation is faster and, as already described in the Theory section, is the most robust since it is able to provide the canonical coefficients even when the x and y variables are almost rank deficient or singular matrices. In particular, such a situation occurs when applying the multi-voxel approach to the edge voxels of the MRSI grid. In fact, 2 rows and 2 columns of dummy voxels need to be introduced. Practically, the additional rows and columns of dummy voxels are simply obtained by producing a copy of the first (last) row of voxels of the original grid at the top (bottom), and a copy of the first (last) column of voxels at the left (right) hand-side of the given grid. In the example under investigation, the resulting grid has dimensions 16×16 instead of 14×14. The dummy voxels allow the application of any multi-voxel spatial model, but the x matrix will now contain some components that are equal to each other (as for the 3×3 model and 3×3 model without corner voxels) or linearly dependent (symmetric 3×3 model), thereby resulting in a singular matrix. The CCA implementation based on Eq. [7] is not able to provide a solution, since the computation of the inverse of the matrix C_{xx} is not possible. The implementation CCA-GEP based on solving the symmetric generalized eigenvalue problem (Eq. [8]) is able to provide a solution, but it may not be accurate since the matrix C_{xx} has a high condition number. Such problems are overcome by the implementation CCA-PA based on computing principal angles, which then yields the most robust results. As final result, in Fig. 7, the nosologic images obtained by the symmetric 3×3 model (left) and the single voxel model (right), when considering a high noise level, with SD equal to 80×10^6, are shown. The PCA subspace model was used. The images clearly show that the multi-voxel approach significantly

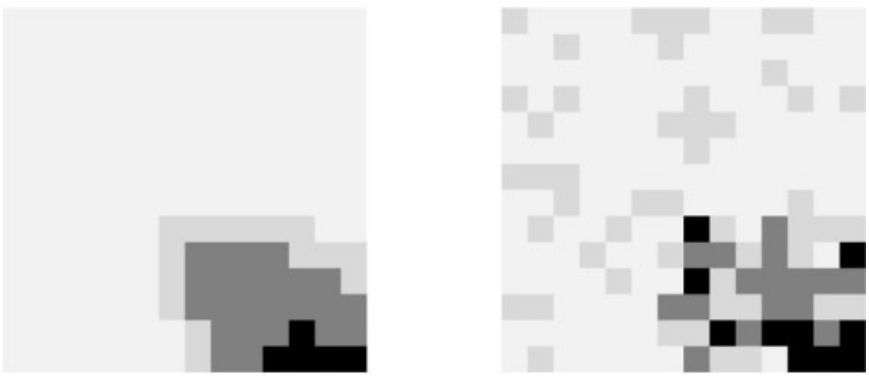


FIG. 7. Nosologic images obtained by the symmetric 3×3 multi-voxel model (left) and the single voxel model (right), for a noise SD equal to 80×10^6. Subspace model: PCA. Black region: aggressive tumor voxels; dark gray region: moderately aggressive tumor voxels; gray region: mixed tissue voxels; light gray: healthy tissue voxels.

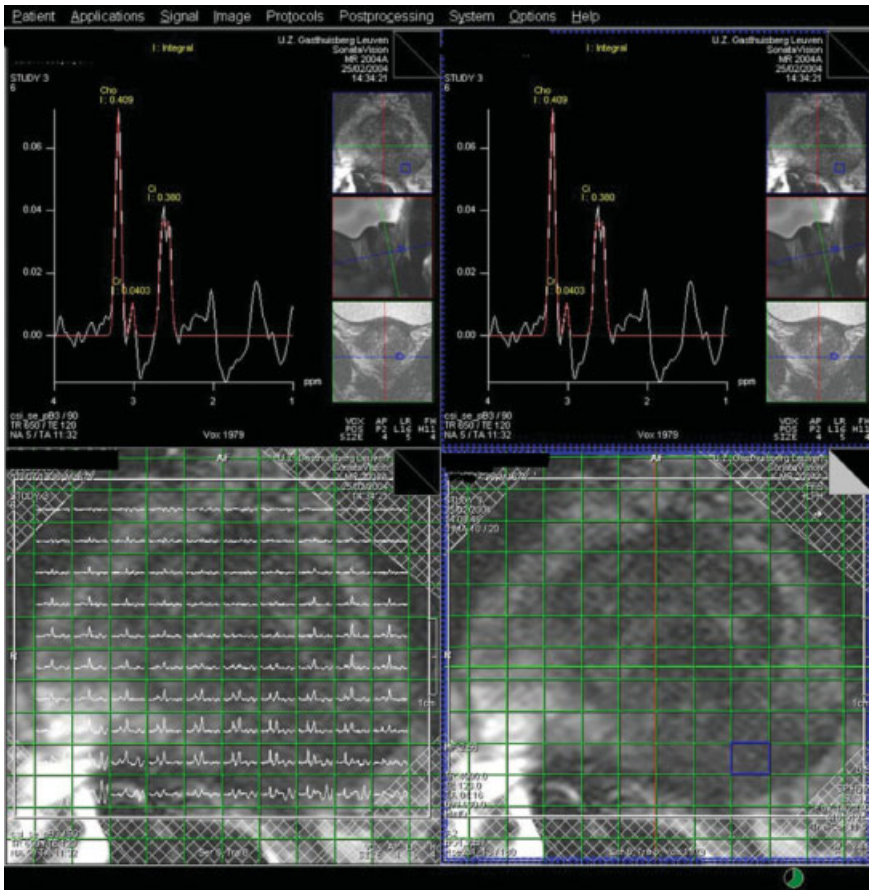


FIG. 8. Screenshot provided by the Siemens scanner for the in vivo prostate MRSI data set.

outperforms the ordinary correlation analysis approach. In fact, the tissue regions detected by CCA are well localized, despite their irregular edges. On the other hand, the single voxel approach detects the presence of aggressive tumor and mixed tissue voxels in parts of the grid where other types of tissue spectra were originally inserted.

In Vivo Results

Figure 8 shows a screenshot, provided by the Siemens scanner, in which the spectral map characterizing the 10×10 PRESS box region, as processed by the spectroscopy package of the Siemens scanner (Syngo MR 2004), is displayed. The saturation blocks used to suppress unwanted fat signals around the prostate are displayed as well. In the prostate image, the suspicious zone is the dark region in the right bottom part. The screenshot also shows the spectrum of the MRS signal characterizing voxel number 88 (in the PRESS box region, the voxels are numbered from the upper left corner to the lower right corner). The spectrum clearly shows a high level of Choline and a low contribution of Citrate. On the basis of the spectroscopy, the following voxels in the neighborhood can be labeled as tumor voxels: 78, 87, 89, 97, 98, and 99. The signals characterizing the MRSI data set contain the following compounds: lipids (between 1 ppm and 2 ppm), Citrate doublet (2.6 ppm), Creatine (3 ppm), Choline (3.2 ppm), and water resonance (4.7 ppm). In order to improve the performance of the proposed tissue segmentation procedure, the signals

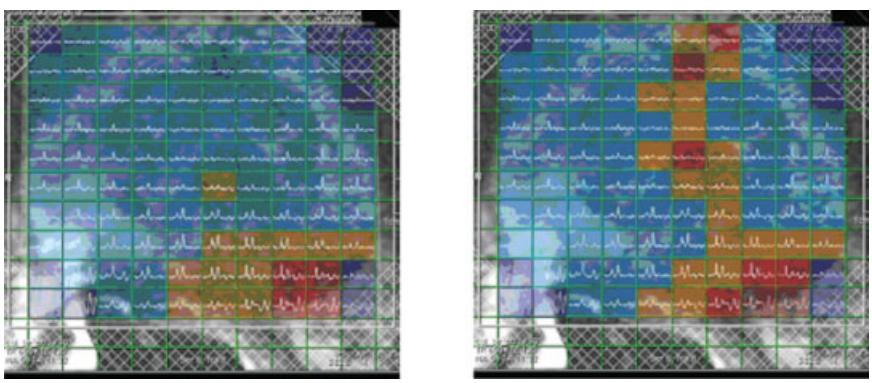


FIG. 9. Nosologic images obtained by processing an in vivo MRSI data set. Left: CCA (spatial model: symmetric 3×3; subspace model: Taylor). Right: ordinary correlation analysis. Brown region: aggressive tumor voxels; red region: moderately aggressive tumor voxels; orange region: mixed tissue voxels; light blue region: healthy tissue voxels, dark blue region: unprocessed voxels.

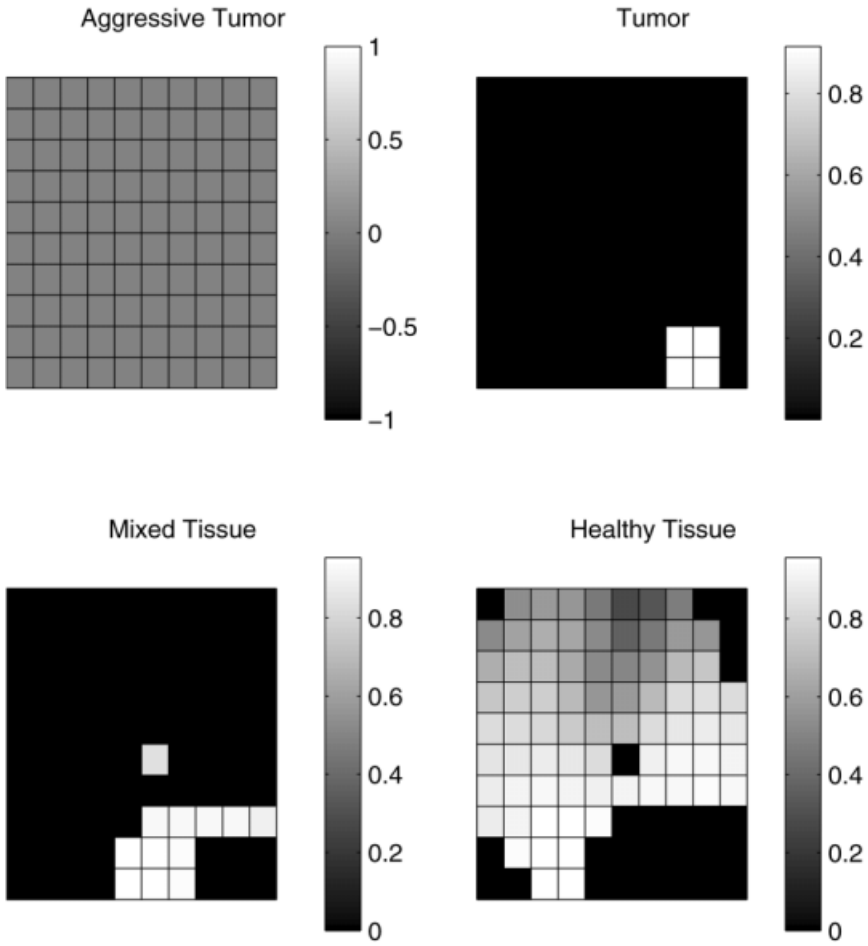


FIG. 10. Canonical coefficient maps obtained for the in vivo MRSI data set by CCA (spatial model: symmetric 3 × 3; subspace model: Taylor) .

were preprocessed by filtering out the water and lipid components. The water and lipid removal was performed by means of HLSVD-PRO (13), which is an improved variant of the popular HLSVD method (14). CCA was then applied to the grid of filtered signals, in order to retrieve the possible tissue types characterizing the sample under investigation. As for the simulation studies, the spatial model as well as the subspace model had to be defined. As far as the spatial model, i.e., the *x* variable, is concerned, the best performance was obtained by applying the symmetric 3 × 3 model. For the subspace model, i.e., the *y* variable, the Taylor approach was adopted. The first component of *y* was defined as the average of 2000 spectra containing the following variations of the noiseless simulated signal parameters: up to 0.05 ppm for the frequencies, up to 40 times the original value of the damping factors, and up to 20% of the original values of the amplitudes.

Figure 9 shows the detection results obtained by applying CCA (left) as well as the results provided by ordinary correlation analysis (right), i.e., the single voxel model. In the nosologic images, the colors denote the tissue types as follows: the brown color denotes the aggressive tumor region, the red color represents the moderately aggressive tumor region, the orange color denotes the mixed tissue region, and the light blue color corresponds to the healthy tissue region. In both images, some dark blue voxels can be observed as well. They correspond to voxels that have not been processed by the segmentation techniques since they are covered by the saturation blocks used for fat suppression around the prostate (see the spectral map in Fig. 8). As can be observed, CCA is able to well localize the suspicious tumor part, while the single voxel model detects as tumor/mixed tissue a much broader region. In particular, some tumor voxels are detected on the upper part of the grid.

In Figs. 10 and 11, the canonical coefficient maps obtained by CCA and the single voxel model, respectively, are visualized for each tissue type. The maps show that the canonical coefficients provided by CCA are significantly bigger than the coefficients provided by the single voxel approach, which points out that the spectra contained in the voxels detected by CCA correlate best with the chosen model spectra, i.e., with the first component of the *y* variable. As further evaluation of the performance of the two approaches, for each tissue region, the correlation coefficient between the spectrum obtained as an average of the spectra contained in the detected voxels and the model spectrum was computed. In Fig. 12 the aforementioned spectra are displayed. The obtained values, reported in Table 2, show a high level of correlation for both methods. However, CCA provides better results for the tumor and mixed regions.

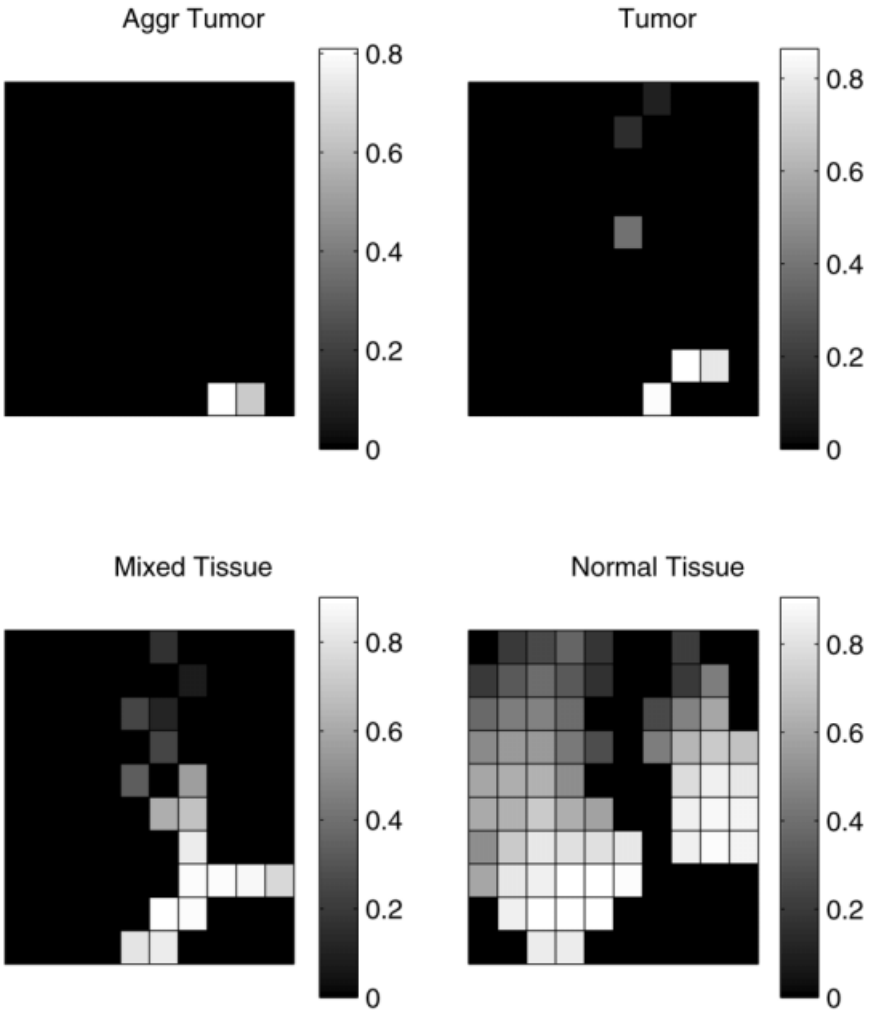


FIG. 11. Canonical coefficient maps obtained for the in vivo MRSI data set by ordinary correlation analysis.

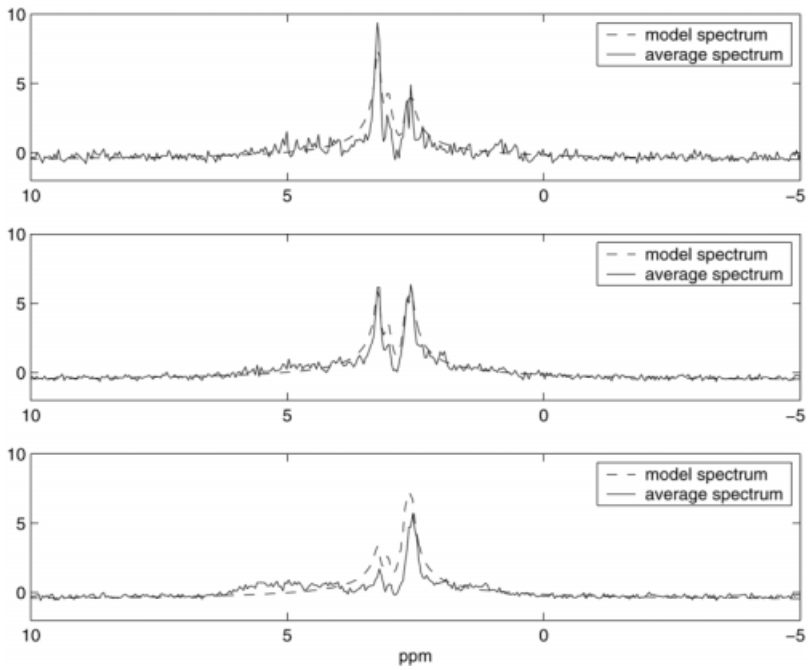


FIG. 12. Model and average magnitude spectra for aggressive tumor (top), mixed tissue (middle), and normal tissue (bottom) obtained by applying CCA to the in vivo MRSI data set. Spatial model: symmetric 3 × 3. Subspace model: Taylor.

Table 2
Correlation Coefficients Between the Average Spectrum and the Model Spectrum for Each Detected Tissue Region

Correlation coefficients	Aggressive tumor	Tumor	Mixed tissue	Healthy tissue
Taylor symmetric 3 × 3	ND*	0.8464	0.9459	0.8581
Single voxel	0.8129	0.8047	0.8850	0.8697

*ND = not detected (no aggressive tumor voxels have been detected).

CONCLUSIONS

CCA is a statistical technique that quantifies the relationship between multivariate random vectors. Our studies show that it can be successfully applied to MRSI data sets since it fully exploits the spatio-spectral nature of this type of biomedical data. In particular, CCA can be applied to MRSI data in order to retrieve in an efficient and accurate way the possible tissue types characterizing the organ under investigation. Extensive simulation and in vivo studies show that CCA significantly outperforms the ordinary correlation analysis, especially for signals with a low Signal to Noise Ratio.

ACKNOWLEDGMENTS

The authors would like to thank O. Friman for providing useful material and information on the application of CCA to biomedical data. Dr. Sabine Van Huffel is a full professor at the Katholieke Universiteit Leuven, Belgium.

REFERENCES

1. Sahoo PK, Soltani S, Wong AKC. A survey of thresholding techniques. Computer Vision, Graphics and Image Processing 1988;41:233–260.
2. Mangin JF, Frouin V, Bloch I, Regis J, Lopez-Krahe J. From 3D magnetic resonance images to structural representations of the cortex topography using topology preserving deformations. Journal of Mathematical Imaging and Vision 1995;5:297–318.
3. Coleman GB, Andrews HC. Image segmentation by clustering. Proceedings of the IEEE 1979,5:773–785.
4. Held K, Kops ER, Krause BJ, Wells WM, Kikinis R, Muller-Gartner HW. Markov random field segmentation of brain MR images. IEEE Transactions on Medical Imaging 1997;16:878–886.
5. Bezdek JC, Hall LO, Clarke LP. Review of MR image segmentation techniques using pattern recognition. Med Phys 1993;20:1033–1048.
6. Reddick WE, Glass JO, Cook EN, Elkin TD, Deaton RJ. Automated segmentation and classification of multispectral magnetic resonance images of brain using artificial neural networks. IEEE Trans Med Imaging 1997;16:911–918.
7. Friman O. Adaptive analysis of functional MRI data, Ph.D. thesis, Dept. Biomed. Engin., Linköpings Univ., Sweden, 2003.
8. Szabo De Edelenyi F, Rubin C, Estève F, Grand S, Décorps M, Lefournier V, Le Bas JF, Rémy C. A new approach for analyzing proton magnetic resonance spectroscopic images (^{1}H MRSI) of brain tumors: nosologic images. Nature Medicine 2000;6:1287–1289.
9. Hotelling H. Relation between two sets of variates. Biometrika 1936;28: 321–377.
10. Golub GH, Zha H. In: Bojanczyk A, Cybenco G, editors. Linear algebra for signal processing. New York: Springer; 1995. p 59–82.
11. Zha H. The singular value decomposition theory, algorithms and applications, Ph.D. thesis, Pennsylvania State University, University Park, PA, 1993.
12. Golub GH, Reinsch C. Singular value decomposition and least squares solutions. Numerical Mathematics 1970;14:403–420.
13. Laudadio T, Mastronardi N, Vanhamme L, Van Hecke P, Van Huffel S. Improved Lanczos algorithms for blackbox MRS data quantitation. Journal of Magnetic Resonance 2002;157:292–297.
14. Pijnappel WWF, van den Boogaart A, de Beer R, van Ormondt D. SVD-based quantification of magnetic resonance signals. Journal of Magnetic Resonance 1992;97:122–134.